Coastal Engineering 200 (2025) 104752

Contents lists available at ScienceDirect

Coastal Engineering

journal homepage: www.elsevier.com/locate/coastaleng

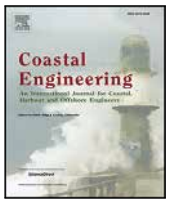

SBI: A sandbar extraction spectral index for multi-spectral satellite optical imagery

Salomé Frugier [a,*], Rafael Almar [a], Erwin Bergsma [b], Alice Granjou [a]

[a] LEGOS (IRD/CNRS/Toulouse University/CNES), Toulouse, France
[b] EOlab, CNES, Toulouse, France

ARTICLE INFO

Keywords:
Satellite-derived sandbar position
Sentinel-2
Sandbar dynamic
NOM
SBI (SandBar Index)

ABSTRACT

Satellite imagery allows for large-scale monitoring of dynamic coastal processes, with shoreline tracking being the most widespread application. Nearshore wave-generated sandbars influence coastal dynamics by acting as natural buffers that reduce beach erosion through wave energy dissipation and sediment exchange with the aerial beach. Despite their importance, they are often overlooked in satellite-based studies. This paper addresses this oversight by introducing the SandBar Index (SBI), a new methodology designed to optimize the detection of wave breaking pixels induced by the underlying sandbar while minimizing the SBI value pixels from the surrounding environment such as sand, land and water. Wave breaking pixels refer to image pixels where breaking waves generate foam, increasing reflectance in optical satellite imagery. Since wave breaking typically occurs over submerged sandbars, these pixels act as proxies for their detection. By integrating this index into an automated processing framework, long-term time series of sandbar positions are generated alongside shoreline positions. To validate our methodology, Sentinel-2 images are used to compare satellite-derived sandbar positions with in-situ bathymetric data from the Field Research Facility (FRF) in Duck, North Carolina (US), over a period of nearly ten years. Validation results show good agreement (STD = 23.2 m - i.e. 2 Sentinel-2 pixels), demonstrating the ability of the method to capture the onshore and offshore migration of sandbars. The flexibility of the SBI allows implementation on different satellite platforms, including Landsat and VENμS, demonstrating its transferability. This application lays the groundwork for future studies using over 40 years of historical satellite data to further investigate long-term sandbar dynamics, but also high-frequency dynamics with the concomitantly increasing revisit and resolution of satellite missions. The integration of multiple observable metrics from satellite data allows for a more nuanced characterization of the coastal system as a dynamic entity.

1. Introduction

Sandy coasts are dynamic and vulnerable areas increasingly exposed to hazards due to intensified oceanographic forcing (Li et al., 2018; Barnard et al., 2017; Harley et al., 2017; Masselink et al., 2016) and human activities (Dada et al., 2023). Within the nearshore zone, sandbars—particularly subtidal ones—form and evolve as a result of wave breaking and currents (Wright and Short, 1984). These sandbars are subject to constant sediment reorganization, driven by physical processes in both transverse and longitudinal directions (Ribas et al., 2017). The variability in hydrodynamics leads to significant changes in coastal bathymetric profiles (Plant et al., 1999; Walstra et al., 2016), highlighting the importance of monitoring these submerged features.

Continuous monitoring of sandbars is important for coastal management because their different forms (longitudinal, transverse, crescentic) can dissipate wave energy through successive breaking, thereby reducing coastal erosion during storms. Depending on their shape, they can protect the shoreline, the beach face, or the nearshore zone from high wave energy impacts. The number, spacing, and shape of these bars are influenced by factors such as the slope of the surf zone, sediment grain size, tidal range, wave energy and direction, and sediment supply (Price et al., 2014; Dubarbier et al., 2015; Splinter et al., 2018). However, their nearshore topography is complex, and their position and variability are important for both short- and long-term beach stability (Lippmann and Holman, 1990). This knowledge also informs beach safety, such as the prediction of rip currents, and is relevant for navigation, including boat landings for example.

Wright and Short's (Wright and Short, 1984) classification scheme, widely used for single-bar coasts, identifies six beach states based

* Corresponding author at: LEGOS (IRD/CNRS/Toulouse University/CNES), Toulouse, France.
E-mail address: salome.frugier@ird.fr (S. Frugier).

https://doi.org/10.1016/j.coastaleng.2025.104752
Received 29 November 2024; Received in revised form 17 February 2025; Accepted 31 March 2025
Available online 13 April 2025

on the morphology of sandbars. These states range from the 2D dissipative state under high-energy conditions (D) to 3D forms under intermediate conditions (Longitudinal Bar and Trough, LBT, Rhythmic Bar and Beach, RBB, and Transverse Bar and Rip, TBR, Low Tide Terrace, LTT), and the 2D reflective state under low-energy waves (R). During high-energy conditions, sandbars can migrate offshore rapidly (O(10 m/day)), leading to beach erosion (Wright and Short, 1984; Thornton et al., 1996). Conversely, during low-energy periods, bars might migrate onshore slowly (O(1 m/day)), resulting in beach accretion (Hoefel and Elgar, 2003). The dynamic sandbar migration are influenced by the complex impacts of climate change, including increased storm frequency and extreme events. These processes can accelerate coastal erosion while promoting the formation and offshore migration of sandbars, emphasizing the need for continuous monitoring. However, limited data availability remains a challenge, as long-term coastal monitoring programs based on in situ measurements are restricted to a few sites worldwide (e.g., Pianca et al. (2015), Turner et al. (2016))

To monitor the positions of submerged sandbar crests, several methods have been widely used, ranging from seasonal and annual data collected through echo sounding (Tătui et al., 2016; Yuhi et al., 2016) to LiDAR surveys (Aleman et al., 2017), satellite imagery (Lafon et al., 2004), X-band radar (Ruessink et al., 2002), and video techniques (Almar et al., 2010; Lippmann and Holman, 1990). In situ measurements often have spatial limitations, are time-consuming and resource-intensive, and are frequently hampered by the challenging and potentially dangerous conditions of the surf zone (Almar et al., 2010). However, the nearshore zone offers many exploitable optical signatures, such as wave breaking, which manifests as bright patches of foam on the water's surface. Since waves generally break in shallow waters, areas where foam is concentrated can serve to locate submerged sandbars (Lippmann and Holman, 1989). However, long-exposure videos offer limited spatial (longitudinal) and temporal coverage, making it difficult to process sandbar dynamics over long distances along the coastline (i.e., several tens of kilometers) or across temporal scales ranging from a few days to several seasons.

The increasing access to Earth observation data, particularly multispectral satellite imagery, presents a solution for obtaining long-term observations of coastal transformations over the past three decades in various locations worldwide. In particular, the emergence of Google Earth Engine (Gorelick et al., 2017) has greatly facilitated access to the growing archive of publicly available satellite images, enabling global analyses extending back decades, with data now acquired at least every 5 days (Donchyts et al., 2016; Li et al., 2019; Luijendijk et al., 2018; Mentaschi et al., 2018). The applications of satellite imagery have so far primarily been limited to shoreline detection (Gens, 2010; Vos et al., 2019b; Almar et al., 2023) and bathymetry derived from coastal satellites (Chybicki, 2017; Almar et al., 2021, 2022). Sandbars are often overlooked in studies, even though they play an important role in coastal dynamics and beach protection, influencing erosion and accretion processes, and thus directly related to the shoreline (Pianca et al., 2015; Ribas et al., 2017). Few studies today still use satellite images to detect sandbars. To date, there are primarily manual extraction approaches (Athanasiou et al., 2018; Rodríguez-Martín and Rodríguez-Santalla, 2013), while automatic methods remain rare in the literature (Tătui et al., 2016; Do et al., 2021; Janušaitė et al., 2021).

Román-Rivera and Ellis (2019), in their review of coastal bar detection via remote sensing, cite several earlier studies (Lee et al., 1999; Lafon et al., 2004; Klemas, 2011; Holman and Haller, 2013; Monteys et al., 2015), but automatic extraction remains a challenge. Janušaitė et al. (2021) proposes a fully automated algorithm based on a GIS for extracting the morphological features of sandbars in images from PlanetScope and RapidEye satellites. Aside from the work of Janušaitė et al. (2021) and Tătui et al. (2016), using very high-resolution (VHR) satellite images, no other study to date addresses the automatic extraction of sandbar positions using publicly available HR satellite data such as Sentinel-2 or Landsat. The radiometric resolution for the VHR satellites is often limited to red, green, blue, and a NIR band in some cases, and thus the spectral indices for VHR satellites are mostly a multiplication of the three visible bands (blue, green, and red), combined with a methodology similar to that used to estimate water depth (Stumpf et al., 2003).

The method proposed is not computationally expensive and can examine local beaches or any around the world from any laptop with a connection to the internet. Long-term satellite missions, such as Landsat and Sentinel-2, can provide over 40 years of freely accessible medium-resolution optical imagery, enabling in-depth coastal studies at different spatio-temporal scales. Thus, the objectives of our study are to develop a new spectral index, the SandBar Index (SBI), which maximizes the pixels of white foam while minimizing those of other environments (land, sand, and water) along perpendicular profiles to the coast. Furthermore, the automatic extraction process of sandbar positions are explained through the analysis of wave breaking patterns, addressing the steps of preprocessing, detection, and extraction. This method is then validated using Sentinel-2 satellite images. The discussion section addresses the limitations of this approach and its transferability to other optical satellite sensors, including the Landsat and VENμS satellites, followed by the conclusions.

2. Study area

Located on the northern Outer Banks of North Carolina, FRF-site is a prominent site for coastal monitoring, recognized internationally for its long-term data collection. Since 1981, extensive bathymetric surveys have been conducted at intervals ranging from biweekly to monthly, covering a 1-kilometer stretch of shoreline from the surf zone to the dune. These surveys are performed using specialized amphibious vehicles such as the Coastal Research Amphibious Buggy (CRAB) or the Lighter Amphibious Resupply Cargo (LARC) vehicle with RTK-GPS and an acoustic sensor (Birkemeier and Mason, 1984; Forte et al., 2018).

The research conducted at FRF-site has shown that sandbar dynamics are episodic (Lippmann et al., 1993), with sandbars migrating offshore during short, intense periods of elevated wave heights, significantly above the annual average (Anderson et al., 2023). However, not every storm that meets these criteria results in a change in the sandbar state (Ruessink et al., 2009), reflecting the complexity of sandbar dynamics and the influence of storm conditions on coastal morphology. This site, characterized by a microtidal regime, is located on the exposed eastern coastline of the United States, where coastal processes are influenced by relatively small tidal ranges. A local coordinate system is defined for the facility, with the y-axis oriented alongshore with a 18.2° counterclockwise from true north and the origin located at the southern edge of the property (36.1776° N, 75.7497° W).

3. Methods

3.1. Formulation of the SandBar index (SBI)

An index is generated by combining spectral bands from a single acquisition. Physically, each illuminated object has a unique reflective signature across the electromagnetic spectrum. By selecting the appropriate combination of spectral bands, an index enhances the visibility of certain features, making them stand out more clearly in the image. This is the principle behind how indices function, as they help to differentiate specific objects within a scene. Spectral water indices are used in remote sensing to distinguish land pixels from water pixels. Primarily used for shoreline detection, they help monitor coastal changes such as beach accretion and erosion. The NDWI (Normalized Difference Water Index) (Gao, 1996) and the MNDWI (Modified NDWI) (Xu, 2006) leverage reflectance differences in near-infrared, green, and short-wave infrared bands to enhance water detection. The AWEI (Automated Water Extraction Index) and its variant AWEIsh

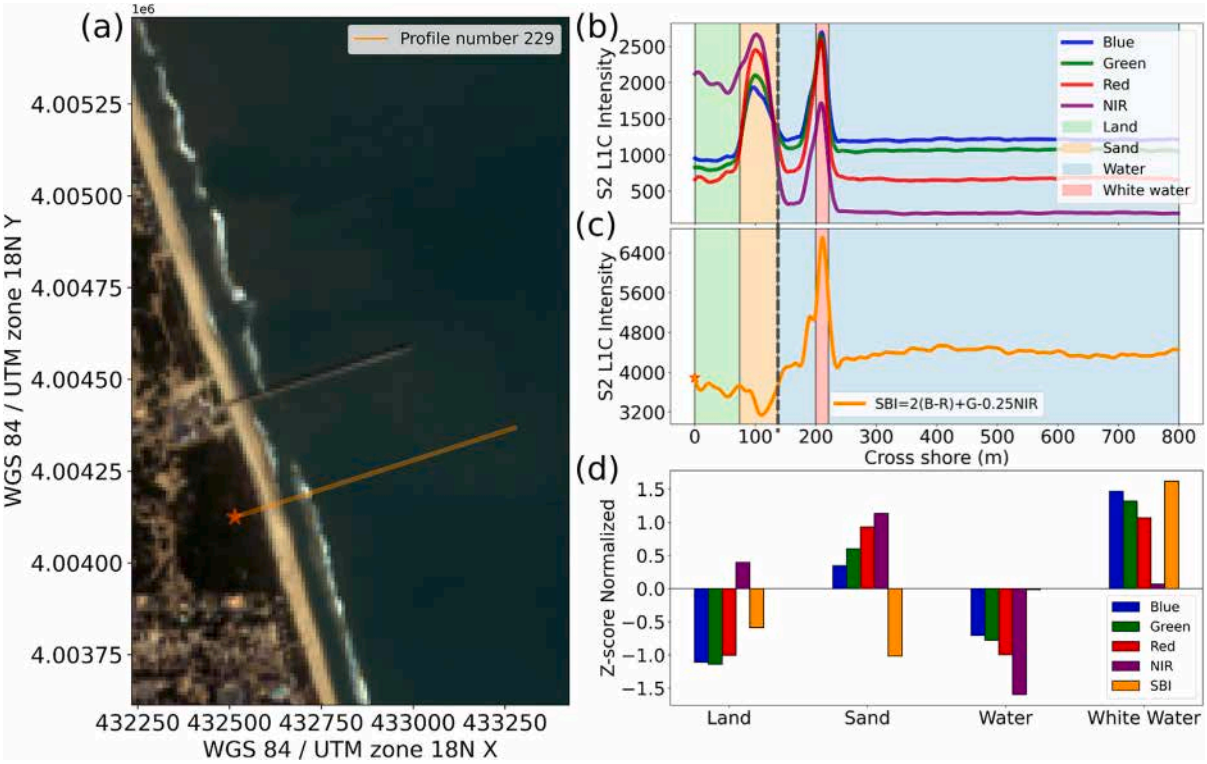

Fig. 1. **(a)** Sentinel-2 acquisition at FRF-site, on October 7, 2022. **(b)** Cross-shore coastal spectral response of the blue, green, red and NIR bands, and **(c)** SandBar Index (SBI). The shoreline is indicated by a gray dashed line. **(d)** Comparison of SBI estimated values (orange) with the four bands (blue, green, red, and NIR) over the four intertidal environments: land, sand, water, and white-water.

(AWEI for Shadow) (Feyisa et al., 2014) further improve water classification in complex environments by reducing interference from built-up areas and shadows. Sandbars, which influence wave dynamics and sediment transport, are often obscured by breaking waves, making their identification challenging. the foam created by these waves can serve as a visual marker, as waves break upon the sandbars when present. In fact, Lippmann and Holman (1989) demonstrated that wave breaking patterns can reveal sandbar positions. The proposed spectral index focuses on identifying foam pixels relative to other land cover types.

To ensure broad applicability, the index is built using the four spectral bands common to most multispectral satellites: blue, green, red, and near-infrared (NIR). This choice allows compatibility across sensors, as not all satellites include shortwave infrared (SWIR) bands. For instance, while Landsat and Sentinel-2 have SWIR bands, the VENμS satellite, despite its high spatial resolution (4–5 m) and 2-day revisit frequency, does not include SWIR.

The index is defined using multiple linear regression applied to spectral data from fifty Sentinel-2 images that capture areas with active wave action and white-water foam. Spectral responses are recorded across four classified zones: “land”, “sand”, “water”, and “white-water”. Regression analysis determines optimal coefficients that maximize the spectral response of white-water. The result is an optimized spectral index, named the SandBar Index (SBI), specifically designed to highlight white foam areas, and minimize other (land, sand and water):

$$\mathrm{SBI} = 2 \times (\mathrm{B} - \mathrm{R}) + \mathrm{G} - 0.25 \times \mathrm{NIR} \tag{1}$$

B, R, G, and NIR represent the reflectance values of the respective spectral bands: blue, red, green, and near-infrared. The coefficients in the equation have been rounded to make the index more user-friendly. The linear regression is not site-specific; the same coefficients can be used for all sites.

Fig. 1**(a)** presents a Sentinel-2 acquisition at FRF-site, in Duck, North Carolina (US), with a cross-shore profile corresponding to profile number 229 from the local coordinate system. The cross-shore profile is indicated by a solid orange line, with the origin located at the profile’s starting point on land, marked by a red star. Fig. 1**(b)** shows the spectral responses of the four bands along this profile, also highlighting the four different environments: land, sand, water and white water.

In the land zone, the blue, green, and red bands display relatively consistent average radiance (~850), while the NIR band shows significantly higher radiance (~2700). Near the sand zone, the radiance of all bands increases due to the higher reflectance of sand. However, in the water zone, the NIR band is nearly zero (~200) due to strong absorption, while the visible bands decrease but maintain moderate values (~1000). This absorption, particularly in the NIR range, contributes to the distinct spectral behavior observed in water. In the white-water zone, characterized by breaking waves, the blue, green, and red bands exhibit high radiance (~2500), while the NIR band shows a relatively high radiance of about ~1700. Notably, the blue and green bands consistently show higher radiance in aquatic zones than the red band, which exhibit higher values on land.

Fig. 1**(c)** displays the spectral response after applying the SBI index along the same profile demonstrating the maximization of white water pixels while minimizing those from other environments. Furthermore, the histogram in Fig. 1**(d)** shows that pixels corresponding to land and sand are significantly reduced, while the response in the water zone is largely unaffected, as the radiance in this area was already low. However, the white-water pixels show a clear increase, reflecting the SBI index’s ability to identify the breaking wave foam pixels.

Normalization is applied using the 90th percentile of the data rather than the absolute maximum because it can be influenced by outliers, such as excessive reflections or sensor errors, which do not represent typical conditions. By focusing on the 90th percentile, the impact of these outliers is minimized, ensuring that the normalization process accurately reflects the typical range of values in the image. The result is a Normalised SandBar Index (NSBI):

$$\mathrm{NSBI} = \frac{\mathrm{SBI} - \mathrm{SBI}_{min}}{\mathrm{SBI}_{90} - \mathrm{SBI}_{min}} \tag{2}$$

Normalization of the index is applied because satellites like Landsat, VENμS, and Sentinel-2 exhibit similar responses to different environments along a cross-shore profile but produce different values. This step enhances the reliability of the spectral index across various satellite systems.

3.2. Sandbar position extraction

An adaptable algorithm has been developed to automatically extract sandbars at decameter resolution from multispectral satellite images. It has been tested specifically on pre-processed Sentinel-2 images to demonstrate its capabilities. The process begins with pre-processing the satellite image, followed by local downloading via platforms like Google Earth Engine and Theia. Once downloaded, the NSBI is calculated using Eqs. (1) and (2). The analysis begins by extracting NSBI values along all cross-shore profiles from local system coordinate. To support sandbar detection, the shoreline position is also determined using the SCoWI (Subtractive Coastal Water Index), as outlined in Bergsma et al. (2024). By combining the NSBI with the SCoWI, the algorithm offers a more robust method for locating sandbars and provides insight into their position relative to the shoreline.

3.2.1. Pre-processing

Google earth engine. This section outlines the use of Google Earth Engine (GEE) for pre-processing and downloading images, as well as identifying products suitable for coastal detection. GEE is an online geospatial computing platform developed by Google that facilitates large-scale analysis of satellite images and geospatial datasets (Gorelick et al., 2017). It provides access to a vast archive of historical and current satellite images along with powerful data processing tools, supporting environmental research and natural resource management. The Python API of GEE is used to download satellite images, allowing convenient access to publicly available Top Of Atmosphere (TOA) reflectance images from various collections, as detailed by Chander et al. (2009). NASA offers images with a 30-meter resolution and a 16-day revisit frequency through Landsat 5 (TM), 7 (ETM+), 8 (OLI), and 9 (OLI-2) satellites, which provide reliable spectral reflectance and geometric precision. Similarly, the European Space Agency (ESA) offers Sentinel-2 images with a 10-meter resolution and a 5-day revisit period, classified as Level-1C, equivalent to Landsat's Tier 1. While other satellites, such as Landsat 1 to 3, exist, their 80-meter resolution or discontinuous records are unsuitable for coastal studies (Vos et al., 2019a). Thus, all Tier 1 TOA satellite images from Landsat 4, 5, 7, and 8 collections, along with Sentinel-2 Level-1C scenes covering the study sites is retrieved. GEE is particularly valuable for our sandbar detection process, as it allows selective downloading of only the region of interest (ROI) from satellite images, reducing storage requirements. For calculating the SBI, only the blue, green, red, and near-infrared (NIR) spectral bands are downloaded. For Landsat 7, 8, and 9 data, the available panchromatic band is used to enhance the spatial resolution of the spectral bands from 30 meters to 15 meters through a data fusion method based on principal component analysis (Tu et al., 2001). This fusion allows for more detailed analysis for sandbar detection. In contrast, Landsat 5 (TM) lacks a panchromatic band, so bilinear interpolation is applied to downsample the 30-meter spectral bands to 15 m. To further refine data quality, a cloud cover threshold is applied using GEE's built-in tools. However, this threshold applies to the entire satellite image, which may lead to rejecting images that are cloud-free in the ROI. To address this, all images are included with overall cloud coverage below 90% in our analysis and apply a custom function developed by Graffin et al. (submitted to Communications Earth & Environment) to filter out images with cloud cover specifically within the ROI (see Fig. 2). In addition to cloud interference, another challenge arises from the presence of skyglint. Skyglint happens when the satellite's field of view aligns with scattered sunlight from the atmosphere, creating bright spots or streaks that can distort the image data and lead to additional outliers.

Theia. In addition to using Google Earth Engine (GEE) for Landsat and Sentinel-2 images, VENμS (Vegetation and Environment monitoring on a New Micro-Satellite), a joint mission between the French (CNES, French Space Agency) and Israeli (ISA, Israel Space Agency) space agencies, is retrieved via the Theia platform, a French data distribution service developed by CNES and hosted by the CESBIO (Space Biosphere Agency). Since VENμS is not available on GEE, Theia is used to download Level-1C VENμS images, which provide a 5-meter spatial resolution with a 2-day revisit frequency. These high-resolution images are particularly suited for monitoring coastal environments. Theia's platform allows easy access to VENμS data, ensuring reliable geometric precision and spectral reflectance, making it an important complement to our Landsat and Sentinel-2 datasets for coastal detection.

3.2.2. Sandbars detection and extraction

Satellite-derived position. The sandbar satellite-derived position extraction process starts with using an existing network of cross-shore profiles from the local coordinate system, as the objective is to validate the SBI sandbar detection method. For each cross-shore profile, NSBI values are extracted. Data were then interpolated to 2 m resolution oriented to the cross-shore direction of the local coordinate system and smoothed with a length scale of 30 m to remove noise associated with sensor and other small-scale variations. Without this step, directly analyzing the NSBI profiles would yield sandbar positions that appear coarse and pixelated, directly linked to the resolution limitations of the satellite's optical imagery.

To identify sandbar positions, peaks within the NSBI values are detected without strict thresholds, just a prominence value is set (prominence = 0.2), enabling the algorithm to filter out minor fluctuations and noise. This process ensures that only distinct peaks are identified.

At the FRF-site, the beach alternates between single-bar and double-bar systems. During energetic wave conditions, the inner sandbar undergoes net offshore migration (NOM) (Anderson et al., 2023), moving seaward. In some cases, the high-energy conditions also generate a new sandbar closer to the shore, leading to the formation of a double-bar system.

Fig. 3**(a)** illustrates the detection across all profiles while Fig. 3**(b)** shows an example of the NSBI values along profile number 274 on December 29, 2017, highlighting detected peaks corresponding to wave breaking positions. In wave-dominated coasts, shore breaking can be mistaken for sandbar-induced breaking. To remove this ambiguity, NSBI detections within 40 m of the shoreline are excluded, with this threshold being adjustable based on site-specific conditions. Shoreline positions are determined using the method developed by Bergsma et al. (2024), specifically designed for sandy beaches. This approach combines a newly developed multispectral index (SCoWI) with Otsu's threshold refinement method to derive sub-pixel shoreline positions (Otsu, 1979). Fig. 3**(b)** also illustrates an example where a point is excluded due to its proximity to the shoreline.

Fig. 4 demonstrates how the wave breaking detected peaks are classified. In this case, waves are breaking on both sandbars. The method classifies the first breaking peak as shore break, as it occurs within the 40-meter buffer zone. The second peak, being closest to the shore, corresponds to the inner bar, while the third, the farthest from the shore, is attributed to the outer sandbar. When more than two sandbars are present, the method applies the same logic.

In situ position. The sandbar in situ positions are identified using the elevation anomaly, which is defined as the difference between each profile and the median profile over the entire Sentinel-2 period. This approach serves to detrend the signal, making it easier to identify peaks. Indeed, some sandbars do not present obvious peaks, and so harder to detect directly from an elevation profile. First, the data were interpolated to 2 m resolution oriented to the cross-shore direction of the local coordinate system. Once the elevation anomaly is calculated, the global maximum is identified—potentially multiple maxima in the

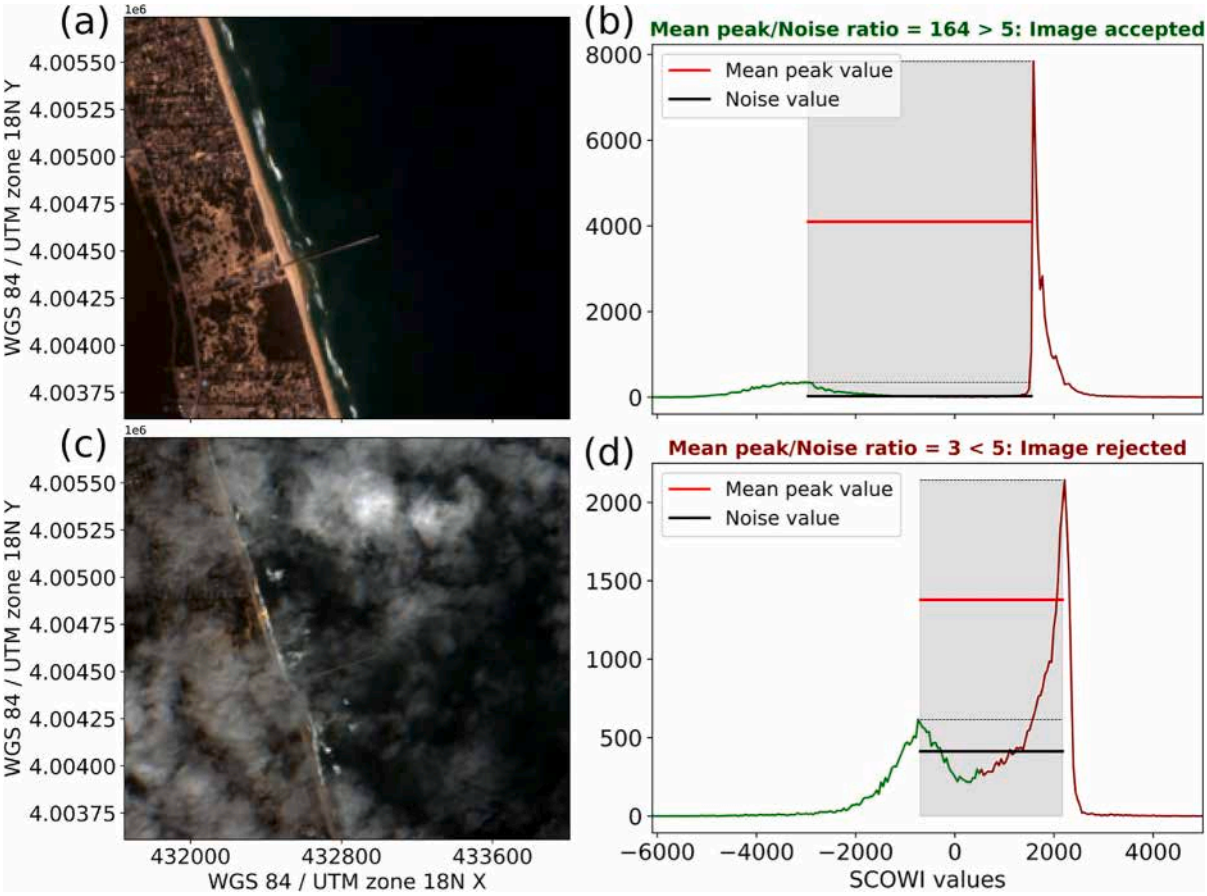

Fig. 2. Image filtering based on cloud coverage at FRF-site, modified after Graffin et al. (submitted to Communications Earth & Environment). The Sentinel-2 acquisition is shown both **(a)** without and **(c)** with cloud coverage, accompanied by the corresponding SCoWI value histograms **(b)** and **(d)**. The mean peak value (solid red line) represents the average of occurrences at both the land-pixel mode peak and the sea-pixel mode peak. The noise value (solid black line) represents the average of all SCoWI values occurring between the two peaks. If the ratio between the mean peak and the noise value falls below 5, the image is discarded.

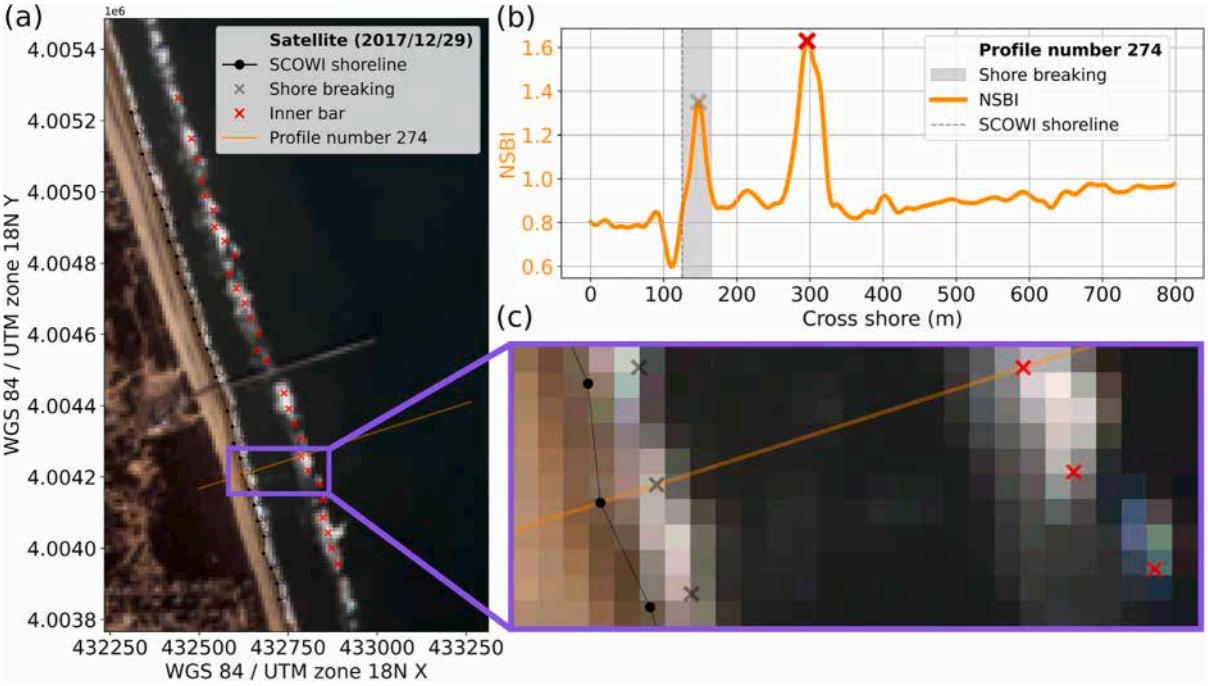

Fig. 3. **(a)** Sentinel-2 acquisition at FRF-site, on December 12, 2017. **(b)** Cross-shore coastal spectral response of the NSBI, where the cross-shore zero origin corresponds to the local coordinate origin at profile number 274. **(c)** Detection area zoom.

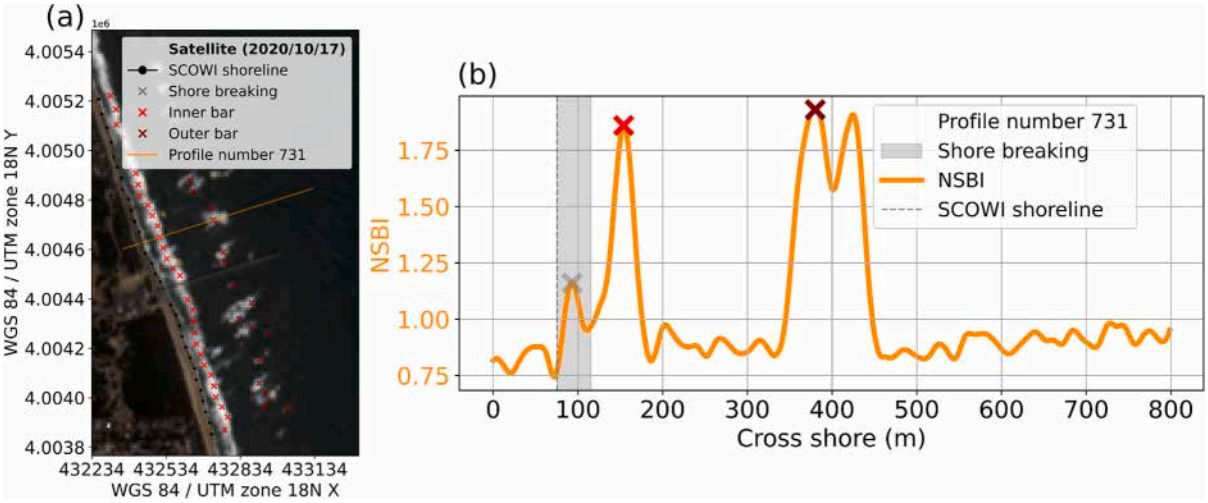

Fig. 4. **(a)** Sentinel-2 acquisition at FRF-site on October 17, 2020. **(b)** Cross-shore coastal spectral response of the NSBI, where the cross-shore zero corresponds to the local coordinate origin at profile number 731.

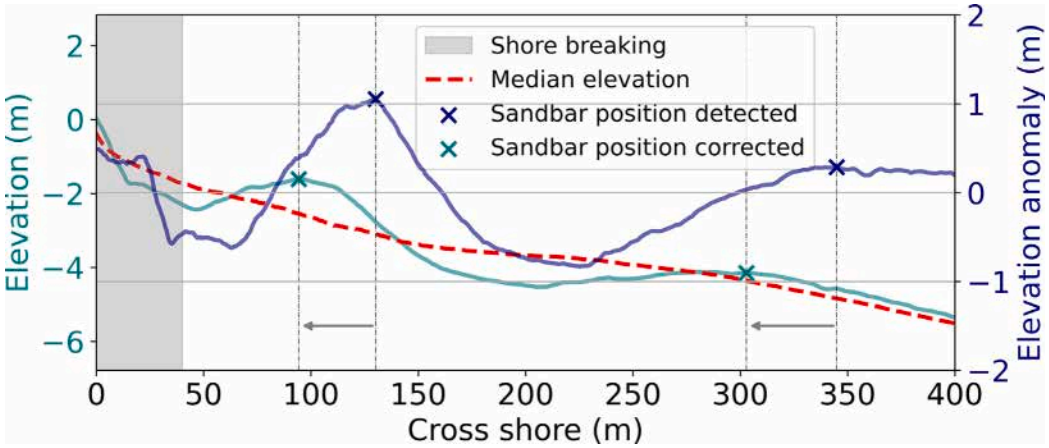

Fig. 5. In situ sandbar position detection using elevation anomaly method and correction based on elevation profile for profile 274 on January 18, 2024, where the cross-shore zero corresponds to the NAVD88 reference elevation.

case of a double-bar system. However, the position detected on the elevation anomaly does not precisely correspond to the actual sandbar position, as there is often an offshore offset in the cross-shore direction. To correct for this, the detected position is mapped back onto the original elevation profile, and its cross-shore position is adjusted to align with the local maximum. The Fig. 5 illustrates an example from January 18, 2024, for profile number 274, where the offshore offset can exceed 40 m.

4. Validation

The validation focuses on the Sentinel-2 period, spanning nearly ten years from July 26, 2015, to November 17, 2024, during which 819 images were acquired. To improve the analysis, a cloud-filtering function developed by Graffin et al. (submitted to Communications Earth & Environment) is applied, reducing the number of usable images to 610. For validation, a dual approach is used: single-date validation to assess performance at specific times and time-series validation to evaluate accuracy over time.

4.1. Single date validation

For the single-date validation, the satellite-derived sandbar position is compared to the in situ position within a window of ± two days. Two examples of a double-bar system are provided in Fig. 6. Figs. 6**(a)** and **(c)** show the performance of the automated detection method for two satellite dates, separated by two days, alongside in situ measurements. Figs. 6**(b)** and **(d)** illustrate an example of cross-shore NSBI intensity profile and the local bathymetry along profile 274. Clearly, there are local maxima in the NSBI intensity distribution in the vicinity of the shoreline and the bar(s).

Fig. 6**(b)** shows wave breaking on both sandbars whereas Fig. 6**(c)** shows breaking only on the inner bar. Comparing the elevation of the outer bar in Figs. 6**(b)** and 6**(d)**, it is found at −2 m and -4 m, respectively, suggesting that the outer bar is too deep for waves to break on it. For additional information, the instantaneous water level is shown as a horizontal dashed blue line. The reference of 0 m is relative to the North American Vertical Datum of 1988 (NAVD88). To obtain the instantaneous water level, the NAVD88 reference was first converted to Mean Sea Level (MSL), and the instantaneous tidal height corresponding to the time of satellite image acquisition was then added. The correction to convert NAVD88 to MSL is 0.128 m and the tidal levels, with a 1-hour temporal resolution, were obtained from the NOAA tide gauge station in Duck, North Carolina (ID 8651370; NOAA (2025)).

In the first example, where wave breaking occurs on both the inner and outer sandbars, the broader wave breaking area leads to less precise detection of the sandbar position, resulting in higher STD value for

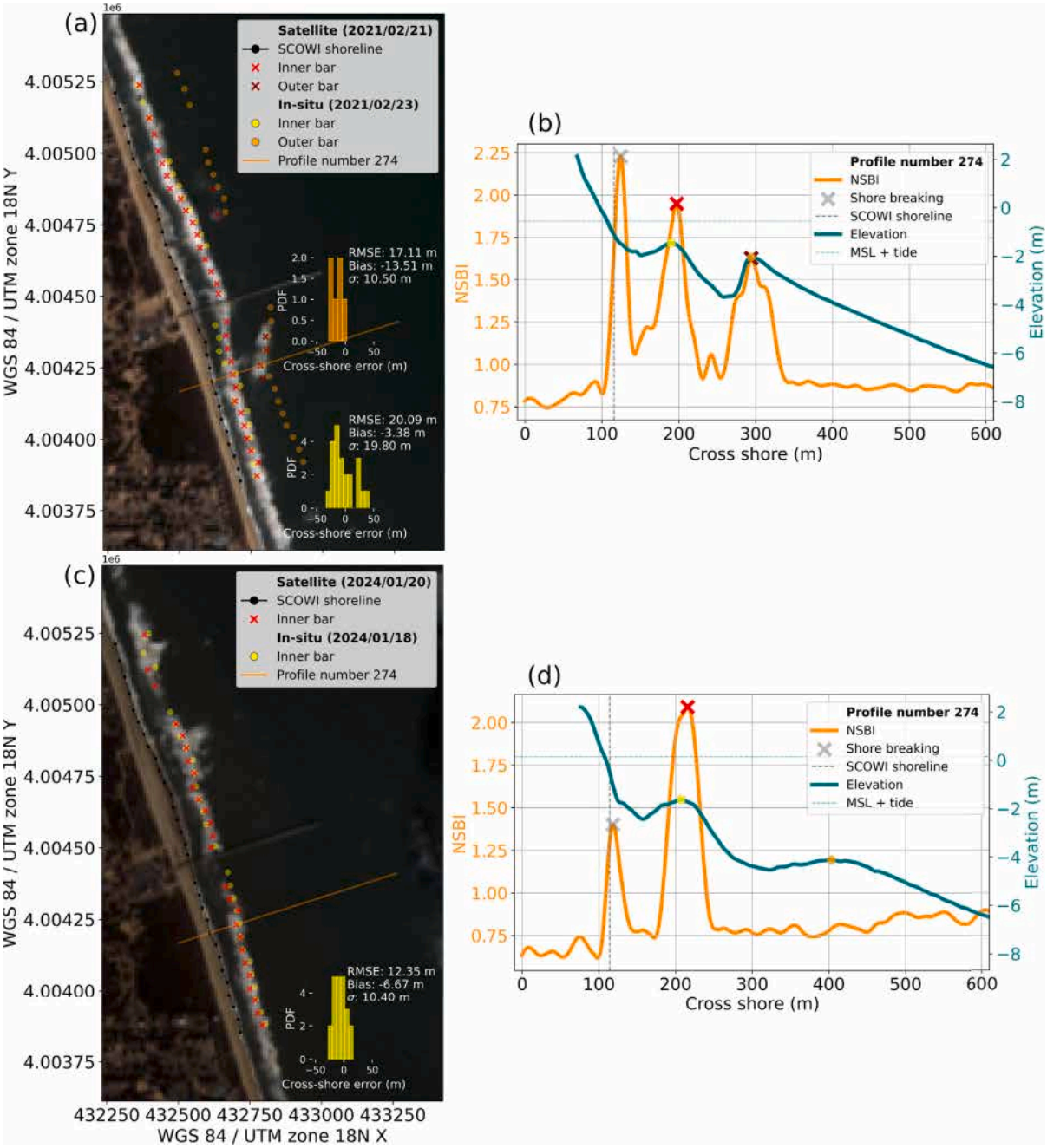

Fig. 6. Sentinel-2 acquisition at FRF-site (**(a)** February 21, 2021 and **(c)** January 20, 2024). Cross-shore NSBI intensity and bathymetry, where the cross-shore zero corresponds to the local coordinate origin at profile number 274 (**(b)** and **(d)**, respectively).

the inner bar (STD = 19.8 m). This wider dissipation zone spreads the intensity peak over a larger area, reducing cross-shore positional accuracy. Conversely, the outer bar experiences less wave breaking overall, but when wave breaking does occur, it tends to be more localized. This localized breaking improves precision, as the satellite image captures the event more accurately, with less spread and less uncertainty in the intensity peak (STD = 10.50 m). In the second example, where wave breaking occurs on the inner bar, the results show better performance (STD = 10.40 m).

Despite the overall reasonable accuracy of the sandbar position relative to ground-truth data, a consistent negative bias is observed, with satellite-derived sandbar positions generally located closer to the shore than in situ measurements. Such a negative bias is not uncommon and may be attributed to wave breaking dynamics. The sandbar crest positions, determined using the SBI index based on the peak intensity of white-water foam, can differ from in situ measurements by a varying distance over time. This distance typically ranges around 10 meters and depends on factors such as offshore wave height, water level, and bathymetry (van Enckevort and Ruessink, 2001). Given the spatial resolution of 10 m, this discrepancy may not be significant in the context of satellite-based monitoring, but it remains an aspect that should be better understood and addressed in future research endeavors. Additionally, this example highlights the necessity of excluding points detected too close (within 40 m) to the shoreline from being classified as sandbars, as the bathymetry clearly demonstrates that these points do not correspond to submerged sandbar features but only shore-break.

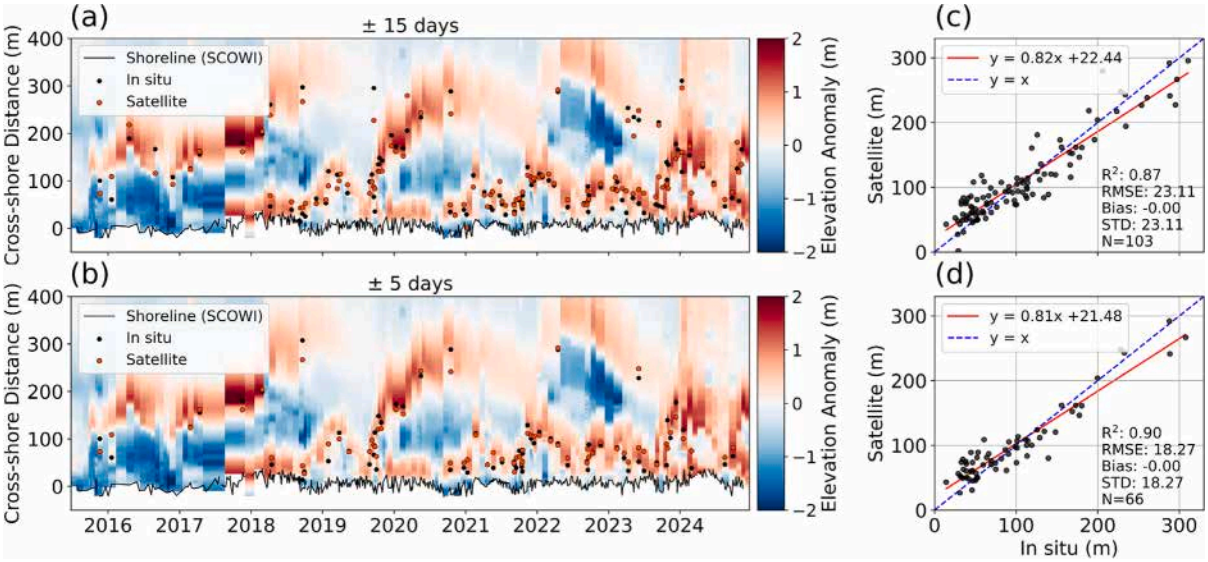

Fig. 7. Validation plots showing the comparison between satellite-derived and in situ sandbar positions for the cross-shore profile number 914 from the local coordinate system. On each row, the top and bottom panels represent the sandbar position time series with **(a)** ±15 days window and **(b)** ±5 days window. R^2, RMSE, STD and bias are shown in (**(c)** and **(d)**, respectively). Note that the higher positive values correspond to the seaward direction, and the cross-shore zero corresponds to the first shoreline of the time series detected by SCoWI.

4.2. Time series validation

To complement the spatial validation on certain dates, a temporal validation is done. The ±2 day window is extended to ±15 days, increasing the validation points number. Outliers are removed using the Interquartile Range (IQR) method, which identifies and excludes data points that fall significantly outside the central range of the dataset. Specifically, the IQR is calculated as the difference between the third quartile (Q3) and the first quartile (Q1), and values lying beyond 1.5 times the IQR from these quartiles are considered outliers. This step filter out images contaminated by cloud or skyglint that may introduce anomalous values, as they can have a similar spectral response to white foam. However, since these anomalies can appear in areas where wave breaking is not possible, the IQR method effectively removes them. Nonetheless, some outliers may still persist, but they are accounted for in the validation of the method.

The positions of sandbars derived from in situ data are compared with those obtained from satellite observations. Fig. 7**(a)** illustrates an example of results along profile number 914. The elevation anomaly highlights the emergence of new sandbars near the shore, followed by their migration into deeper waters. This movement often occurs in the form of episodic jumps, where the bars shift to greater distances from the shore. However, this migration pattern exhibits considerable temporal variability, with different bars emerging and disappearing at varying times (Anderson et al., 2023). In situ sandbar positions are shown in black, while those derived from satellite data are represented in red. The correlation of these 103 points shows a bias centered at 0, indicating that the RMSE is equal to the STD of 23.11 m.

In Fig. 7**(b)**, the effect of reducing the window to ±5 days is also examined. This naturally results in fewer points for validation but improves precision, with the STD decreasing from 23.11 m to 18.27 m. Ultimately, regardless of the window size, the precision remains within approximately two Sentinel-2 pixels (i.e., 20 m).

Fig. 8 illustrates a map showing the position of the local beach profiles, color-coded based on their R^2, STD, and the number of validation points. These metrics are derived by comparing satellite-based sandbar positions with in situ sandbar position data. The R^2 value, which averages 0.8 across the profiles, indicates a strong correlation between the two datasets, reflecting the reliability of the satellite data for sandbar position estimation. The average bias for the remaining 29 profiles is centered around zero. This is why only the STD is presented in Fig. 8, as it effectively captures the degree of error dispersion. With an STD equal to 23.19 m, the data are both precise and accurate.

The spatial variability observed in Fig. 8 is interesting, though not immediately obvious. The pier acts as a physical barrier disrupting seasonal alongshore sediment transport, primarily from the south in the summer and from the north in winter. This disruption leads to a seasonal accumulation of sediments on the upstream side of the pier (Pianca et al., 2015). The influence of the pier dominates the local shoreline behavior, creating a balance between sediment transport and accumulation (Miller and Dean, 2007).

Beyond these spatial patterns, the quality of the sandbar detection appears to be related to the number of validation points. As seen in the validation map, profiles with a higher number of points tend to exhibit higher R^2 scores and lower STD values, indicating both greater accuracy and precision.

The validation time series uses windows of ±15 days, meaning the sandbars could have experienced significant displacement within this period. Also, it is important to highlight that Sentinel-2 has a spatial resolution of 10 m, and while the detection method achieves a positional accuracy of approximately 20 m, this remains within an acceptable range considering the spatial scale of the feature and the rapid changes it can undergo (O(10 m/day) under high-energy conditions (Wright and Short, 1984; Thornton et al., 1996) and O(1 m/day) during low-energy periods (Hoefel and Elgar, 2003)). By reducing the time window to 5 days, positional accuracy improves because shorter intervals better capture sandbar positions before significant displacement occurs.

5. Discussion

5.1. Cross-satellite applicability and transferability

While Sentinel-2 now provides a decade of data, its time series remains too short to assess long-term coastal changes. To extend observations over longer periods, other satellites, such as Landsat with over 40 years of archives, can be used. Since the SBI was designed to work with any satellite carrying visible (B, G, R) and NIR bands, its application remains possible across different satellite missions. Like most optical satellites, Sentinel-2, Landsat, and VENμS are sun-synchronous. Over the FRF-site area, they typically pass between 15:10

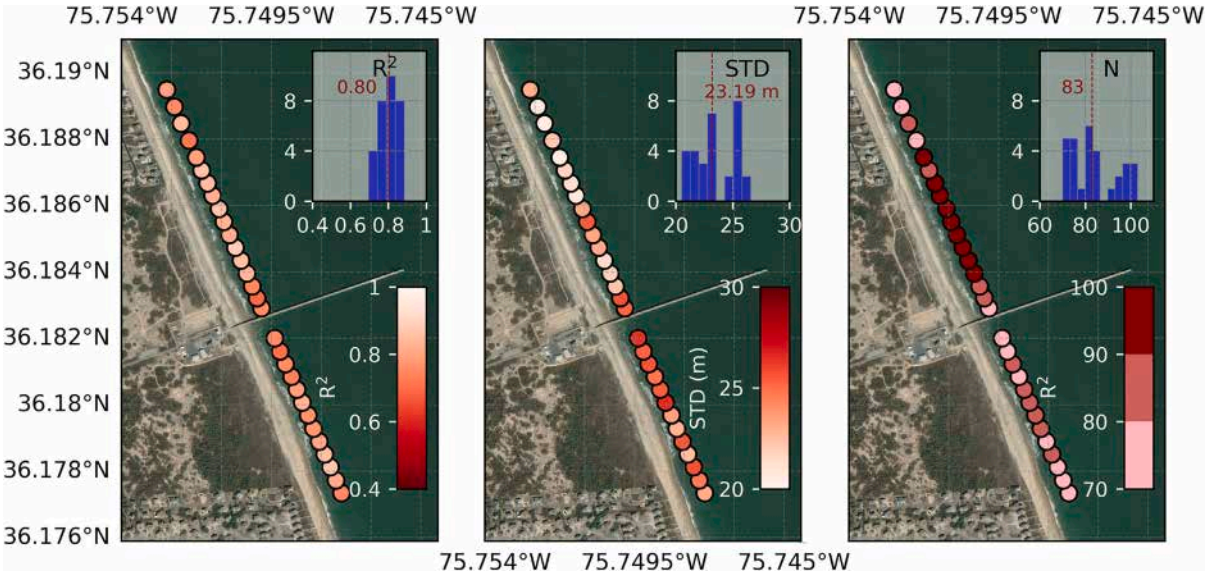

Fig. 8. FRF-site maps showing the 29 validation profile and the validation scores (R^2, STD, and validation points number N) between the time series of cross-shore sandbar position extracted via SBI method and the in situ measurements. On each subplot, the histogram shows the distribution of validation scores.

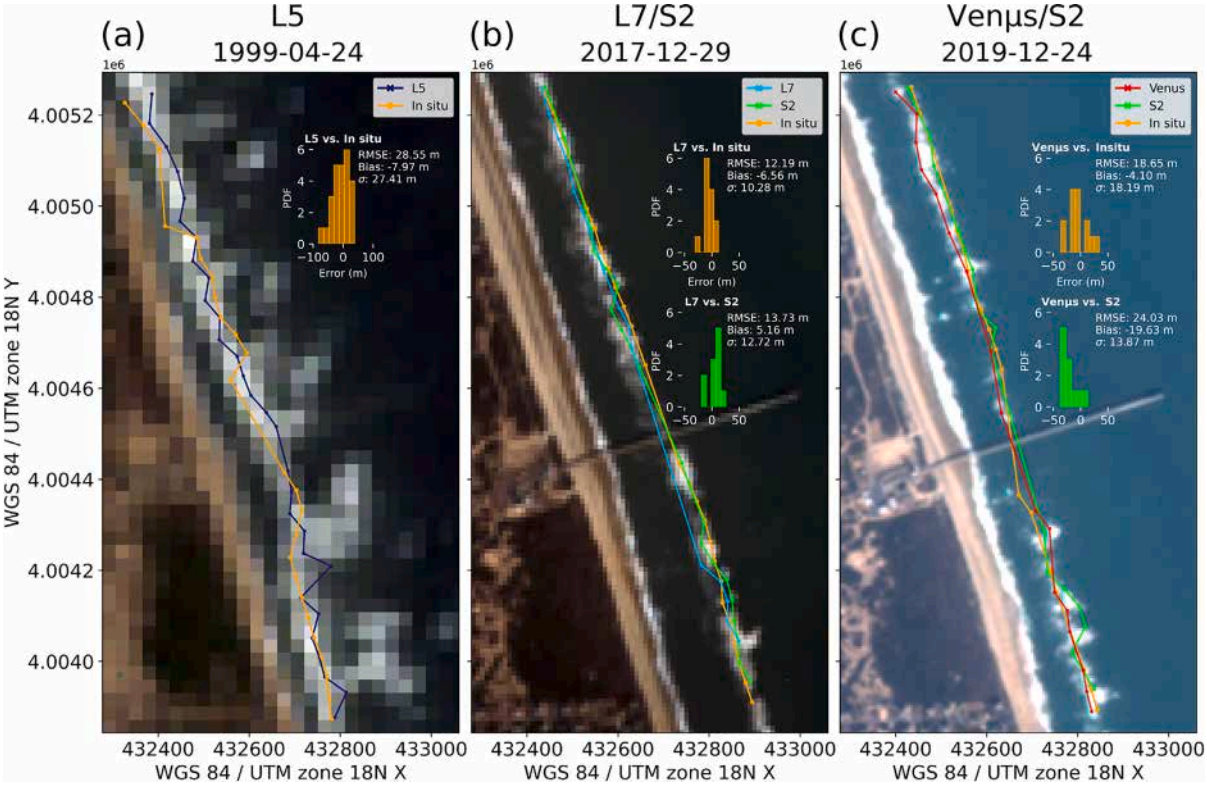

Fig. 9. Showcases the transferability of the SBI index across satellites: **(a)** Landsat 5, **(b)** Landsat 7, and **(c)** VENμS. The orange bars in the histograms display the positional error between the extracted and measured sandbar positions, while the green bars indicate the positional error between the sandbar position extracted from Sentinel-2 and the other satellite.

and 16:10 GMT, with slight variations depending on the specific satellite and orbital cycle. VENμS offers a 2-day revisit, enabling high-frequency coastal monitoring, unlike Sentinel-2 and Landsat. However, its coverage is limited to specific sites and requires a request to CNES. At the FRF-site, it operated from April 4, 2019, to October 17, 2020.

To evaluate the SBI index across different sensors, it is applied to VENμS and Landsat, with the resulting sandbar positions compared to those from Sentinel-2 and the closest in situ data. In some instances, satellites pass over the same area just minutes apart (Fig. 9**b-c**), allowing for direct comparison. For Landsat 5 (1984–2013), no Sentinel-2 images are available, so validation relies solely on in situ data (Fig. 9**a**). Since Landsat 7, 8, and 9 share the same resolution, only a Landsat 7 example is presented. After the Scan Line Corrector (SLC) failure in May 2003, Landsat 7 images exhibit alternating black bands due to data loss, but sandbar detection remains possible (Fig. 9**b**), explaining the gaps in L7-derived positions.

Fig. 9**(b)** shows sandbar detection using Landsat 7 and Sentinel-2 on December 29, 2017, with only a few minutes difference (15:43 and 15:46 GMT). The comparison reveals a seaward bias of 5.2 m and an STD of 12.7 m, with Sentinel-2 positions slightly farther offshore than Landsat 7. When compared to in situ data (December 11, 2017), the Landsat 7 positions show a bias of −6.6 m (towards shore) and an STD of 10.2 m. While the calm wave conditions between December 11 and 29, 2017 (H_s = 0.61 m, T_p = 7.2 s, T_m = 7.0 s, data from the 8 m depth wave gauge) might not entirely account for the observed discrepancy, the STD values suggest that the sandbar detection remains consistent. Fig. 9**(c)** compares the sandbar positions derived from VENμS and Sentinel-2 on December 24, 2019 (15:59 and 15:53 GMT). The analysis reveals a bias of −19.6 m (towards shore) and an STD of 13.9 m, suggesting that VENμS positions are generally closer to the shore, possibly due to its higher resolution (5 m), which might make it more sensitive to variations in sandbar positions. When compared to in situ data (January 10, 2020), the difference shows a bias of −4.1 m (towards shore) and an STD of 18.2 m. The calm to moderate wave conditions (H_s = 0.68 m, T_p = 9.7 s, T_m = 8.2 s) might also not entirely account for the observed discrepancy. Finally, Fig. 9**(a)** presents the difference between Landsat 5 (April 24, 1999) and in situ data (April 19, 1999). The analysis shows a bias of −8 m (towards shore) and an STD of 27.4 m. Despite the relatively calm wave conditions (H_s = 0.59 m, T_p = 5 s), the higher STD compared to the other satellites is likely due to the lower resolution of Landsat 5 (30 m, resharpened to 15 m).

Validation on Landsat 5 and 7 yields STD values of 27 m and 12 m, respectively, which are reasonable considering their lower resolution compared to Sentinel-2, while VENμS, with its higher resolution, achieves an STD of 18 m. The obtained STD values fall within the expected margins, demonstrating the reliability of the sandbar position detection method across different satellite sensors (Lippmann and Holman, 1989). Additionally, by leveraging multiple satellites, it may be possible to improve temporal resolution, offering a more continuous and detailed approach to coastal monitoring.

5.2. Limitations

A major limitation of using satellites for sandbar detection is their inability to capture time-averaged images, unlike video techniques. While sandbar detection has traditionally relied on temporally averaged images from coastal video systems (Lippmann and Holman, 1989; Aarninkhof and Ruessink, 2004), satellites only provide snapshots during wave breaking. This lack of smoothing out individual waves introduces uncertainty, particularly in dynamic environments where sandbar positions can change rapidly over short time scales.

Another key limitation is the absence of wave breaking in calm wave conditions. Without wave breaking over the sandbars, the wave breaking SBI index becomes ineffective, potentially obscuring crucial morphological details of the bars and their interaction with the shoreline. However, alternative methods, such as analyzing water color, may offer useful insights into sandbar positions, even in the absence of breaking waves (Stumpf et al., 2003).

An additional consideration in this context is the exclusion of sandbar detections within 40 meters of the shoreline to mitigate the ambiguity between shore break and sandbar-induced breaking. This threshold was chosen based on site-specific conditions at FRF-site, a microtidal beach, where this distance is appropriate considering the 10 m resolution of the satellite images. However, for larger, macrotidal environments where sandbars are often closer to the shore, this threshold may not be suitable. The 40 m limit is adjustable and could be modified depending on the study site's characteristics. For studies focusing on net offshore migration (NOM) for example, which require the identification of sandbars near the shoreline, this parameter may need further adjustment to ensure the accurate detection of sandbar dynamics.

Furthermore, for this validation, the local coordinate system is used, where profile are spaced approximately 50 meters apart. Increasing the number of profiles improves the detection method. However, the distance between profiles is constrained by the image resolution, as spacing smaller than the resolution would not provide additional value. A finer longshore spacing between profiles will captures the longshore variability of the sandbar. Future analyses could explore transitions between the different beach states as classified by Wright and Short (1984).

Conclusions

This paper demonstrates the potential of the SBI spectral index, specifically designed to maximize wave breaking pixels, for automatically extracting instantaneous sandbar positions from satellite data. By relying solely on physical reflectance, the method is independent of external data, stable across a range of coastal environments, and requires no prior training. Using freely available satellite imagery, specifically Sentinel-2, we validate 10-years sandbar dynamics at the FRF-site in Duck, North Carolina (US). The method shows no systematic bias in sandbar position validation over time, with an accuracy of 23.2 m (STD), approximately two Sentinel-2 pixels, and a strong correlation (R^2 = 0.8), which is consistent with the dynamic nature of sandbars influenced by hydrodynamic wave processes. While this study primarily focuses on Sentinel-2, the method is adaptable to other satellites such as Landsat and VENμS, offering promise for the rapid and stable monitoring of coastal dynamics from the 1980s to the present. However, the effectiveness of this method depends on image quality (spatial and radiometric resolution) and environmental conditions (e.g., water transparency, skyglint, cloud cover, small breaking waves). As satellite resolution improves, this method can be extended to a broader range of coastal sites and temporal scales, yielding valuable insights into long-term coastal dynamics. Additionally, incorporating water color analysis could refine sandbar detection, particularly in non-breaking conditions.

CRediT authorship contribution statement

Salomé Frugier: Writing – original draft, Validation, Software, Methodology, Investigation, Formal analysis, Conceptualization. **Rafael Almar:** Writing – review & editing, Methodology, Conceptualization. **Erwin Bergsma:** Writing – review & editing, Validation, Methodology. **Alice Granjou:** Validation.

Declaration of competing interest

The authors declare that they have no known competing financial interests or personal relationships that could have appeared to influence the work reported in this paper.

Acknowledgments

The authors gratefully acknowledge the individuals and institutions whose contributions made this study possible, particularly the research teams responsible for conducting bathymetric surveys, processing the data, and making it publicly available. This research relied on Sentinel-2 mission data, provided by the European Space Agency (ESA) through the Copernicus Programme of the European Commission. The lead author is supported by a scholarship from the ANR ASTRID programme under the GLOBCOASTS project (N°ANR-22-ASTR-0013). We also thank Spicer Bak and the other anonymous reviewer, and the editor Dr. Marcel van Gent for their valuable comments and suggestions, which significantly improved the manuscript. Any use of trade, firm, or product names is for descriptive purposes only and does not imply endorsement by the U.S. Government. Also, this study has been partially supported through the grant EUR TESS N°ANR-18-EURE-0018 in the framework of the Programme des Investissements d'Avenir.

Data availability

Data will be made available on request.

References

Aarninkhof, S., Ruessink, B., 2004. Video observations and model predictions of depth-induced wave dissipation. IEEE Trans. Geosci. Remote. Sens. 42 (11), 2612–2622, Conference Name: IEEE Transactions on Geoscience and Remote Sensing.

Aleman, N., Certain, R., Robin, N., Barusseau, J.P., 2017. Morphodynamics of slightly oblique nearshore bars and their relationship with the cycle of net offshore migration. Mar. Geol. 392, 41–52.

Almar, R., Bergsma, E.W.J., Brodie, K.L., Bak, A.S., Artigues, S., Lemai-Chenevier, S., Cesbron, G., Delvit, J.-M., 2022. Coastal topo-bathymetry from a single-pass satellite video: Insights in space-videos for coastal monitoring at Duck Beach (NC, USA). Remote. Sens. 14 (7), 1529, Number: 7 Publisher: Multidisciplinary Digital Publishing Institute.

Almar, R., Bergsma, E.W.J., Thoumyre, G., Baba, M.W., Cesbron, G., Daly, C., Garlan, T., Lifermann, A., 2021. Global satellite-Based Coastal bathymetry from waves. Remote. Sens. 13 (22), 4628, Number: 22 Publisher: Multidisciplinary Digital Publishing Institute.

Almar, R., Boucharel, J., Graffin, M., Abessolo, G., Thoumyre, G., Papa, F., Ranasinghe, R., Montano, J., Bergsma, E., Baba, M.W., Jin, F.-F., 2023. Influence of El Niño on the variability of global shoreline position. Nat. Commun. 14.

Almar, R., Castelle, B., Ruessink, B.G., Sénéchal, N., Bonneton, P., Marieu, V., 2010. Two- and three-dimensional double-sandbar system behaviour under intense wave forcing and a meso–macro tidal range. Cont. Shelf Res. 30 (7), 781–792.

Anderson, D., Bak, A.S., Cohn, N., Brodie, K.L., Johnson, B., Dickhudt, P., 2023. The impact of inherited morphology on sandbar migration during mild wave seasons. Geophys. Res. Lett. 50 (3), e2022GL101219, _eprint: https://onlinelibrary.wiley.com/doi/pdf/10.1029/2022GL101219.

Athanasiou, P., de Boer, W., Yoo, J., Ranasinghe, R., Reniers, A., 2018. Analysing decadal-scale crescentic bar dynamics using satellite imagery: A case study at Anmok beach, South Korea. Mar. Geol. 405, 1–11.

Barnard, P.L., Hoover, D., Hubbard, D.M., Snyder, A., Ludka, B.C., Allan, J., Kaminsky, G.M., Ruggiero, P., Gallien, T.W., Gabel, L., McCandless, D., Weiner, H.M., Cohn, N., Anderson, D.L., Serafin, K.A., 2017. Extreme oceanographic forcing and coastal response due to the 2015–2016 El Niño. Nat. Commun. 8 (1), 14365, Publisher: Nature Publishing Group.

Bergsma, E.W.J., Klotz, A.N., Artigues, S., Graffin, M., Prenowitz, A., Delvit, J.-M., Almar, R., 2024. Shoreliner: A sub-Pixel Coastal waterline extraction pipeline for multi-spectral satellite optical imagery. Remote. Sens. 16 (15), 2795, Number: 15 Publisher: Multidisciplinary Digital Publishing Institute.

Birkemeier, W.A., Mason, C., 1984. The crab: A unique nearshore surveying vehicle. J. Surv. Eng. 110 (1), 1–7, Publisher: American Society of Civil Engineers.

Chander, G., Markham, B.L., Helder, D.L., 2009. Summary of current radiometric calibration coefficients for Landsat MSS, TM, ETM+, and EO-1 ALI sensors. Remote Sens. Environ. 113 (5), 893–903.

Chybicki, A., 2017. Sciendo. Pol. Marit. Res. 24 (3), 15–25.

Dada, O.A., Almar, R., Morand, P., Bergsma, E.W.J., Angnuureng, D.B., Minderhoud, P.S.J., 2023. Future socioeconomic development along the West African coast forms a larger hazard than sea level rise. Commun. Earth Environ. 4 (1), 1–12, Publisher: Nature Publishing Group.

Do, J.D., Jin, J.-Y., Jeong, W.M., Lee, B., Kim, C.H., Chang, Y.S., 2021. Observation of nearshore crescentic sandbar formation during storm wave conditions using satellite images and video monitoring data. Mar. Geol. 442, 106661.

Donchyts, G., Baart, F., Winsemius, H., Gorelick, N., Kwadijk, J., van de Giesen, N., 2016. Earth's surface water change over the past 30 years. Nat. Clim. Chang. 6 (9), 810–813, Publisher: Nature Publishing Group.

Dubarbier, B., Castelle, B., Marieu, V., Ruessink, G., 2015. Process-based modeling of cross-shore sandbar behavior. Coast. Eng. 95, 35–50.

van Enckevort, I.M.J., Ruessink, B.G., 2001. Effect of hydrodynamics and bathymetry on video estimates of nearshore sandbar position. J. Geophys. Res.: Ocean. 106, 16969–16979, _eprint: https://onlinelibrary.wiley.com/doi/pdf/10.1029/1999JC000167.

Feyisa, G.L., Meilby, H., Fensholt, R., Proud, S.R., 2014. Automated Water Extraction Index: A new technique for surface water mapping using Landsat imagery. Remote Sens. Environ. 140, 23–35.

Forte, M., Birkemeier, W., Mitchell, J.R., 2018. Nearshore Survey System Evaluation. Coastal and Hydraulics Laboratory (U.S.).

Gao, B.-c., 1996. NDWI—A normalized difference water index for remote sensing of vegetation liquid water from space. Remote Sens. Environ. 58 (3), 257–266.

Gens, R., 2010. Remote sensing of coastlines: detection, extraction and monitoring. Int. J. Remote Sens. 31 (7), 1819–1836, Publisher: Taylor & Francis.

Gorelick, N., Hancher, M., Dixon, M., Ilyushchenko, S., Thau, D., Moore, R., 2017. Google earth engine: Planetary-scale geospatial analysis for everyone. Remote Sens. Environ. 202, 18–27.

Harley, M.D., Turner, I.L., Kinsela, M.A., Middleton, J.H., Mumford, P.J., Splinter, K.D., Phillips, M.S., Simmons, J.A., Hanslow, D.J., Short, A.D., 2017. Extreme coastal erosion enhanced by anomalous extratropical storm wave direction. Sci. Rep. 7 (1), 6033, Publisher: Nature Publishing Group.

Hoefel, F., Elgar, S., 2003. Wave-induced sediment transport and sandbar migration. Science 299 (5614), 1885–1887, Publisher: American Association for the Advancement of Science.

Holman, R., Haller, M.C., 2013. Remote sensing of the nearshore. Annu. Rev. Mar. Sci. 5, 95–113, Publisher: Annual Reviews.

Janušaitė, R., Jukna, L., Jarmalavičius, D., Pupienis, D., Žilinskas, G., 2021. A novel GIS-based approach for automated detection of nearshore sandbar morphological characteristics in optical satellite imagery. Remote. Sens. 13 (11), 2233, Number: 11 Publisher: Multidisciplinary Digital Publishing Institute.

Klemas, V., 2011. Remote sensing techniques for Studying Coastal ecosystems: An overview. J. Coast. Res. 27 (1), 2–17, Publisher: Coastal Education and Research Foundation.

Lafon, V., De Melo Apoluceno, D., Dupuis, H., Michel, D., Howa, H., Froidefond, J.M., 2004. Morphodynamics of nearshore rhythmic sandbars in a mixed-energy environment (SW France): I. Mapping beach changes using visible satellite imagery. Estuar. Coast. Shelf Sci. 61 (2), 289–299.

Lee, Z., Carder, K.L., Mobley, C.D., Steward, R.G., Patch, J.S., 1999. Hyperspectral remote sensing for shallow waters: 2. Deriving bottom depths and water properties by optimization. Appl. Opt. 38 (18), 3831–3843, Publisher: Optica Publishing Group.

Li, H., Wan, W., Fang, Y., Zhu, S., Chen, X., Liu, B., Hong, Y., 2019. A google earth engine-enabled software for efficiently generating high-quality user-ready Landsat mosaic images. Environ. Model. Softw. 112, 16–22.

Li, N., Yamazaki, Y., Roeber, V., Cheung, K.F., Chock, G., 2018. Probabilistic mapping of storm-induced coastal inundation for climate change adaptation. Coast. Eng. 133, 126–141.

Lippmann, T.C., Holman, R.A., 1989. Quantification of sand bar morphology: A video technique based on wave dissipation. J. Geophys. Res.: Ocean. 94, 995–1011, _eprint: https://onlinelibrary.wiley.com/doi/pdf/10.1029/{JC}094iC01p00995.

Lippmann, T.C., Holman, R.A., 1990. The spatial and temporal variability of sand bar morphology. J. Geophys. Research: Ocean. 95, 11575–11590, _eprint: https://onlinelibrary.wiley.com/doi/pdf/10.1029/JC095iC07p11575.

Lippmann, T.C., Holman, R.A., Hathaway, K.K., 1993. Episodic, nonstationary behavior of a double bar system at Duck, North Carolina, U.S.A., 1986–1991. J. Coast. Res. 49–75, Publisher: Coastal Education & Research Foundation, Inc..

Luijendijk, A., Hagenaars, G., Ranasinghe, R., Baart, F., Donchyts, G., Aarninkhof, S., 2018. The state of the world's beaches. Sci. Rep. 8 (1), 6641, Publisher: Nature Publishing Group.

Masselink, G., Castelle, B., Scott, T., Dodet, G., Suanez, S., Jackson, D., Floc'h, F., 2016. Extreme wave activity during 2013/2014 winter and morphological impacts along the Atlantic coast of Europe. Geophys. Res. Lett. 43 (5), 2135–2143, _eprint: https://onlinelibrary.wiley.com/doi/pdf/10.1002/2015GL067492.

Mentaschi, L., Vousdoukas, M.I., Pekel, J.-F., Voukouvalas, E., Feyen, L., 2018. Global long-term observations of coastal erosion and accretion. Sci. Rep. 8 (1), 12876, Publisher: Nature Publishing Group.

Miller, J.K., Dean, R.G., 2007. Shoreline variability via empirical orthogonal function analysis: Part I temporal and spatial characteristics. Coast. Eng. 54 (2), 111–131.

Monteys, X., Harris, P., Caloca, S., Cahalane, C., 2015. Spatial prediction of coastal bathymetry based on multispectral satellite imagery and multibeam data. Remote. Sens. 7 (10), 13782–13806, Number: 10 Publisher: Multidisciplinary Digital Publishing Institute.

NOAA, 2025. Station home page - NOAA tides & currents. https://tidesandcurrents.noaa.gov/stationhome.html?id=8651370.

Otsu, N., 1979. A threshold selection method from gray-level histograms. IEEE Trans. Syst. Man, Cybern. 9 (1), 62–66, Conference Name: IEEE Transactions on Systems, Man, and Cybernetics.

Pianca, C., Holman, R., Siegle, E., 2015. Shoreline variability from days to decades: Results of long-term video imaging. J. Geophys. Res.: Ocean. 120 (3), 2159–2178, _eprint: https://onlinelibrary.wiley.com/doi/pdf/10.1002/2014JC010329.

Plant, N.G., Holman, R.A., Freilich, M.H., Birkemeier, W.A., 1999. A simple model for interannual sandbar behavior. J. Geophys. Res.: Ocean. 104, 15755–15776, _eprint: https://onlinelibrary.wiley.com/doi/pdf/10.1029/1999JC900112.

Price, T.D., Ruessink, B.G., Castelle, B., 2014. Morphological coupling in multiple sandbar systems; a review. Earth Surf. Dyn. 2 (1), 309–321, Publisher: Copernicus GmbH.

Ribas, F., Falqués, A., Garnier, R., 2017. Nearshore sand bars. In: Guillén, J., Acosta, J., Chiocci, F.L., Palanques, A. (Eds.), Atlas of Bedforms in the Western Mediterranean. Springer International Publishing, pp. 73–79.

Rodríguez-Martín, R., Rodríguez-Santalla, I., 2013. Detection of submerged sand bars in the Ebro Delta using ASTER images. In: Huang, Y., Wu, F., Shi, Z., Ye, B. (Eds.), New Frontiers in Engineering Geology and the Environment. Springer, pp. 103–106.

Román-Rivera, M.A., Ellis, J.T., 2019. A synthetic review of remote sensing applications to detect nearshore bars. Mar. Geol. 408, 144–153.

Ruessink, B.G., Bell, P.S., van Enckevort, I.M.J., Aarninkhof, S.G.J., 2002. Nearshore bar crest location quantified from time-averaged X-band radar images. Coast. Eng. 45 (1), 19–32.

Ruessink, B.G., Pape, L., Turner, I.L., 2009. Daily to interannual cross-shore sandbar migration: Observations from a multiple sandbar system. Cont. Shelf Res. 29 (14), 1663–1677.

Splinter, K.D., Harley, M.D., Turner, I.L., 2018. Remote sensing is changing our view of the coast: Insights from 40 years of monitoring at Narrabeen-Collaroy, Australia. Remote. Sens. 10 (11), 1744, Number: 11 Publisher: Multidisciplinary Digital Publishing Institute.

Stumpf, R.P., Holderied, K., Sinclair, M., 2003. Determination of water depth with high-resolution satellite imagery over variable bottom types. Limnol. Oceanogr. 48 (1), 547–556, _eprint: https://onlinelibrary.wiley.com/doi/pdf/10.4319/lo.2003.48.1_part_2.0547.

Tătui, F., Vespremeanu-Stroe, A., Ruessink, G.B., 2016. Alongshore variability of cross-shore bar behavior on a nontidal beach. Earth Surf. Process. Landf. 41 (14), 2085–2097, _eprint: https://onlinelibrary.wiley.com/doi/pdf/10.1002/esp.3974.

Thornton, E.B., Humiston, R.T., Birkemeier, W., 1996. Bar/trough generation on a natural beach. J. Geophys. Res.: Ocean. 101, 12097–12110, _eprint: https://onlinelibrary.wiley.com/doi/pdf/10.1029/96JC00209.

Tu, T.-M., Su, S.-C., Shyu, H.-C., Huang, P.S., 2001. A new look at IHS-like image fusion methods. Inf. Fusion 2 (3), 177–186.

Turner, I.L., Harley, M.D., Short, A.D., Simmons, J.A., Bracs, M.A., Phillips, M.S., Splinter, K.D., 2016. A multi-decade dataset of monthly beach profile surveys and inshore wave forcing at Narrabeen, Australia. Sci. Data 3 (1), 160024, Publisher: Nature Publishing Group.

Vos, K., Harley, M.D., Splinter, K.D., Simmons, J.A., Turner, I.L., 2019a. Sub-annual to multi-decadal shoreline variability from publicly available satellite imagery. Coast. Eng. 150, 160–174.

Vos, K., Splinter, K.D., Harley, M.D., Simmons, J.A., Turner, I.L., 2019b. *CoastSat*: A Google Earth Engine-enabled Python toolkit to extract shorelines from publicly available satellite imagery. Environ. Model. Softw. 122, 104528.

Walstra, D.-J.R., Wesselman, D.A., Van der Deijl, E.C., Ruessink, G., 2016. On the intersite variability in inter-annual nearshore sandbar cycles. J. Mar. Sci. Eng. 4 (1), 15, Number: 1 Publisher: Multidisciplinary Digital Publishing Institute.

Wright, L.D., Short, A.D., 1984. Morphodynamic variability of surf zones and beaches: A synthesis. Mar. Geol. 56 (1), 93–118.

Xu, H., 2006. Modification of normalised difference water index (NDWI) to enhance open water features in remotely sensed imagery. Int. J. Remote Sens. Publisher: Taylor & Francis.

Yuhi, M., Matsuyama, M., Hayakawa, K., 2016. Sandbar migration and shoreline change on the Chirihama Coast, Japan. J. Mar. Sci. Eng. 4 (2), 40, Number: 2 Publisher: Multidisciplinary Digital Publishing Institute.